

# *Geological and hydrological controls on water coproduced with coalbed methane in Liulin, eastern Ordos basin, China*

**Yong Li, Dazhen Tang, Hao Xu, Derek Elsworth, and Yanjun Meng**

## **ABSTRACT**

Significant amounts ( $> 150 \text{ m}^3/\text{day}/\text{well}$ ) of water are currently being extracted from coalbed methane (CBM) wells in Permian–Carboniferous coal in the Liulin area of the eastern Ordos basin, China. Waters coproduced with CBM have common chemical characteristics that can be an important exploration tool because they relate to the coal depositional environment and hydrodynamic maturation of groundwater and can be used to guide CBM development strategies. The CBM production targets of the No. 3 and 4 coal seams from sandstone in the Shanxi Formation and No. 8, 9, and 10 coal seams in the karst of the Taiyuan Formation were deposited in fluvial-deltaic and epicontinental-sea environments, respectively. This paper combines CBM geology, hydrogeology, CBM recovery, and laboratory data to define mechanisms of CBM preservation including the important influence of groundwater. Relevant indices include fluid inclusions as an indicator of the hydraulic connection between the coal seam reservoir and the overlying strata and the ensemble characteristics of total dissolved solids (TDS) contents of water, water production rates, and reservoir temperatures as an indication of the current hydraulic connection. The TDS contents of waters from the No. 3 and 4 and No. 9 and 10 coal seams are double those from the subjacent karst No. 8 coal seam, indicating the important control of fast flow in karst. Low-salinity fluid inclusions from the roof of the subjacent-karst No. 8 coal seam also indicate an enduring hydraulic connection with overlying strata during its burial history. Relatively low current temperatures in the No. 8 (subjacent-karst) coal seam also infer a strong hydraulic

## **AUTHORS**

YONG LI ~ *China University of Geosciences (Beijing), School of Energy Resources, Coal Reservoir Laboratory of National Engineering Research Center of CBM Development and Utilization, Beijing, 100083, People's Republic of China; cugbliyong@gmail.com*

Yong Li is a Ph.D. candidate in petroleum geology, researching gas shales and coalbed methane reservoirs. He currently works as a visiting scholar on coal–rock mechanics in the Department of Energy and Mineral Engineering, G3 Center and Energy Institute, The Pennsylvania State University, United States.

DAZHEN TANG ~ *China University of Geosciences (Beijing), School of Energy Resources, Coal Reservoir Laboratory of National Engineering Research Center of CBM Development and Utilization, Beijing, 100083, People's Republic of China; tang@cugb.edu.cn*

Dazhen Tang is a professor of geology at the School of Energy Resources, China University of Geosciences in Beijing. His research interests include coal and coalbed methane geology, gas shale geology, sedimentology, and reservoir evaluation of oil and natural gas.

HAO XU ~ *China University of Geosciences (Beijing), School of Energy Resources, Coal Reservoir Laboratory of National Engineering Research Center of CBM Development and Utilization, Beijing, 100083, People's Republic of China; xuhao600@163.com*

Hao Xu is an associate professor of geology at the School of Energy Resources, China University of Geosciences in Beijing. He received his Ph.D. in 2008 from the China University of Geosciences in Beijing. He has broad experience in the realm of unconventional gas exploration and exploitation.

DEREK ELSWORTH ~ *Pennsylvania State University, Departments of Energy and Mineral Engineering and of Geosciences; elsworth@psu.edu*

Copyright ©2015. The American Association of Petroleum Geologists. All rights reserved.

Manuscript received August 13, 2013; provisional acceptance November 25, 2013; revised manuscript received December 18, 2013; revised manuscript provisional acceptance April 23, 2014; 2nd revised manuscript received June 18, 2014; final acceptance July 21, 2014.

DOI: 10.1306/07211413147

Derek Elsworth is a professor in the Center for Geomechanics, Geofluids, and Geohazards. His interests are in the areas of computational mechanics, rock mechanics, and in the mechanical and transport characteristics of fractured rocks, unconventional hydrocarbons including coal-gas, tight-gas-shales, and hydrates.

YANJUN MENG ~ *China University of Geosciences (Beijing), School of Energy Resources, Coal Reservoir Laboratory of National Engineering Research Center of CBM Development and Utilization, Beijing, 100083, People's Republic of China; mengyanjun15@126.com*

YanJun Meng is a Ph.D. candidate in petroleum geology, researching coalbed methane reservoirs. His recent work focused on the evaluation of the effect of coalbed methane development in the Liulin area, China.

## ACKNOWLEDGEMENTS

We are grateful to the anonymous reviewers and Michael L. Sweet for their careful reviews and detailed comments. This work was supported by the Major National Science and Technology Special Projects (Grant No. 2011ZX05062-01, 2011ZX05034-01), the National Natural Science Foundation Project (Grant No. 41272175), the Ministry of Land and Resources of the People's Republic of China special funds for scientific research on public causes (Grant No. 201311015-01), and the Fundamental Research Funds for the Central Universities (Grant No. 2652013057). This study would not have been possible without the assistance of the China United CBM Co. Ltd, especially their help in water sampling and providing CBM well production records. In addition, we thank AAPG consulting editor Frances Plant Whitehurst for her keen input on several technical and editorial issues, which led to considerable further improvement.

## EDITOR'S NOTE

Color versions of all figures can be seen in the online version of this paper.

connection and active flow regime. Deuterium concentrations are elevated in the mudstone-bounded No. 9 and 10 coal seams, further confirming low rates of fluid transmission. The gas contents of coal seams from the Taiyuan Formation are higher than those from the sandstone-bounded coal seams in Shanxi Formation, also correlating with low rates of water transmission and low permeability. Conceptual models for these fluvial-deltaic and epicontinental-sea environments that are consistent with geology, gas content, and gas and water production rate histories are of gas-pressure sealing for the Shanxi Formation and hydrostatic-pressure sealing for the Taiyuan Formation. These results confirm the important controls of hydrogeological conditions on the preservation of CBM and the utility of hydrogeological indicators in prospecting for CBM.

## INTRODUCTION

As continuous-type unconventional gas reservoirs, coal reservoirs are saturated with ground water and are strongly affected by hydrodynamics. Coalbed methane (CBM) is a hydrological gas, and the flow of formation water accordingly plays an important role in the maintenance and productivity of CBM reservoirs. Formation water can control and reflect important reservoir characteristics, including gas generation, migration, accumulation, and gas recovery, but it can also lead to problems with the safe disposal of the produced water (Kaiser et al., 1994; Ayers, 2002; Scott, 2002; Van Voast, 2003; Pashin, 2007, 2010; Song et al., 2010; Karacan et al., 2011).

Gas content and reservoir pressure are among the most important controls of CBM recoverability (Kaiser et al., 1991; Scott et al., 1994; Bachu and Michael, 2003), and both are closely connected to the hydrogeology of the CBM basin. Scott (2002) reviewed the major hydrogeological factors that affect the distribution of gas content in several CBM basins in the United States. Hydrogeology can influence the development of regional overpressure that allows more gas to be stored in the coal, the migration of gases to permeability barriers that locally increase gas content, and the removal of gases by water flowing through permeable coal seams or joints (Scott, 2002). Van Voast (2003) demonstrated that the geochemical signature of formation waters is an effective exploration tool in evaluating prospects and choices of exploration targets in six principal coalbed methane-producing basins in the United States.

Hydrodynamic conditions strongly affect CBM preservation and productivity (Cai et al., 2011). Water produced from coal primarily includes bound water that is adsorbed on the coal matrix or

trapped in micropores by capillary forces but also includes free water in pores and fracture systems (Norinaga et al., 1997). Bound water does not appreciably flow, whereas free water is mobile, which results in changes in water head and pressure in fracture systems. Maintaining a balance among the three phases of CBM (adsorbed, dissolved, and free) can facilitate the migration of methane in coal. Stagnant or slow-flowing formation water in coal seams will decrease the diffusion of dissolved gas, and higher hydraulic pressures can prevent gas from desorbing, thus resulting in higher CBM contents (Lamarre, 2003). However, vigorous flow can adversely affect gas accumulation and drive fractionation reactions, thereby depleting the gas in  $^{13}\text{C}$  (Song et al., 2010; Tao et al., 2012).

Production of CBM usually entails the coproduction of formation water with chemical characteristics that can be used as an exploration tool. The quantity and quality of this produced water varies from basin to basin and even within the basin itself. The quality of the produced water depends, in part, on the hardness (the resistance to scratching) of the coal within the formation, and the quantity of water depends on type of coal and the overall production history of the basin. Although it is effectively devoid of sulfate, calcium, and magnesium, the ground water primarily contains sodium and bicarbonate as well as chloride in systems influenced by basinal input (Van Voast, 2003). Fluid inclusions captured in seal rocks of coal seams contain information about hydrocarbon generation and fluid connectivity (Dubessy et al., 2001). Under stable geological conditions, water–rock interaction time increases as the groundwater flows deeper. The additional interaction time increases the degree of formation water mineralization and changes the chemistry of the water. Generally, in shallow strata and water recharge areas, the dissolved solids in groundwater are likely composed of calcium, magnesium, and sulfate, with low total dissolved solids (TDS) values; as water flows from meteoric recharge areas into the interior of the basin, the diversity of the compounds dissolved in the water increases (Hem, 1985; Van Voast, 2003). When the water stagnates due to high formation pressures, the dissolved solids are primarily sodium and chloride (Pashin, 2007). Microbial reduction of dissolved

sulfate seems to drive the sequence of processes that modify the water quality. Bicarbonate is a product of the reduction, and with increased dissolved solid concentrations, calcite and dolomite precipitate because of reduced solubilities of calcium and magnesium. Cation exchange with clay may also deplete the dissolved calcium and magnesium but is probably not necessary to arrive at the final chemical characteristics (Van Voast, 2003). Both the evaluations of prospects and the selection of development targets can be enhanced by understanding the geochemical signature of the water associated with the CBM.

There are wide variations in water production rates from coal in different areas and different formations. The ease of dewatering any CBM depends on whether the coal is permeable, interference from other wells or mines, and connection to an aquifer or meteoric waters. For example, the 420 wells in the Black Warrior basin in Alabama had initial water production rates of 1 to 180  $\text{m}^3/\text{day}/\text{well}$ , averaging 18  $\text{m}^3/\text{day}/\text{well}$  (Pashin et al., 1990). The initial water production rate in the southern Ute Reservation of the San Juan basin in Colorado ranged from 2 to 120  $\text{m}^3/\text{day}/\text{well}$ , with an average rate of 8  $\text{m}^3/\text{day}/\text{well}$  (Rogers and Rogers, 1994), whereas the southern San Juan basin had limited water production (Kaiser et al., 1991). In general, the variations in the amount of water coproduced with CBM wells are caused by differences in the coal rank, thickness, permeability, depth, and depositional environment as well as the duration of production and life span of CBM wells (Flores, 2013).

The Liulin area studied in this paper is located in the middle of the eastern Ordos basin, China (Figure 1), and is one of the key CBM development areas in China, with recoverable gas resources of approximately  $210.83 \times 10^8 \text{ m}^3$  in 72.2  $\text{km}^2$  by 2013. In 1991, CBM exploration and development began in China when the North China Petroleum Bureau began the Deep CBM Exploration project in conjunction with the United National Development Programme. One of the selected target areas was located in the Liulin area. Seven CBM wells were drilled with initial rates of 1000 – 3000  $\text{m}^3/\text{d}$  after hydraulic fracturing (Su et al., 2003). However,

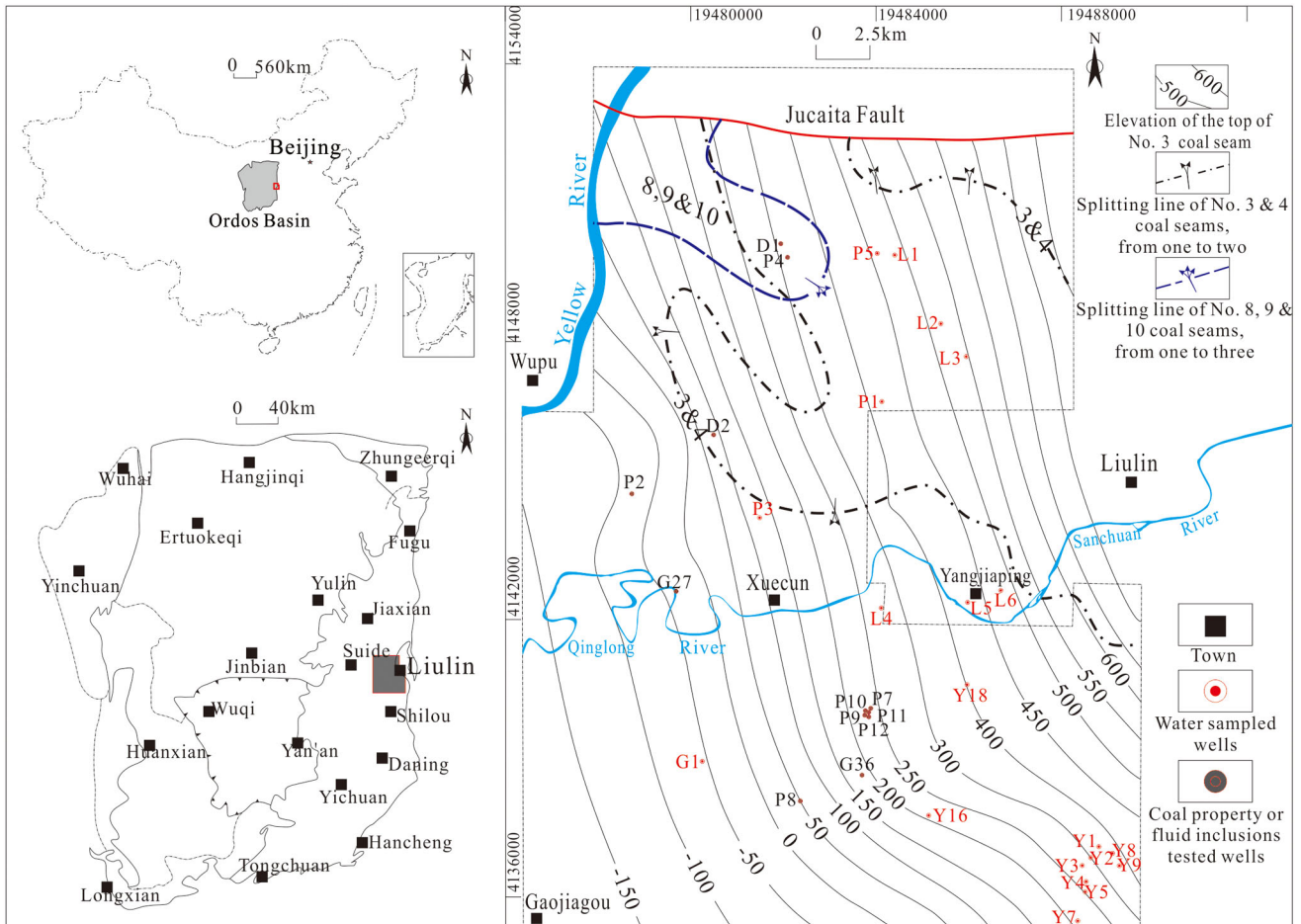


**Figure 1.** Map of the Liulin area in Ordos basin, China. The structural elevation of the top of the No. 3 coal seam and the splitting lines of the No. 3 and 4 and No. 8, 9, and 10 coal seams are shown.

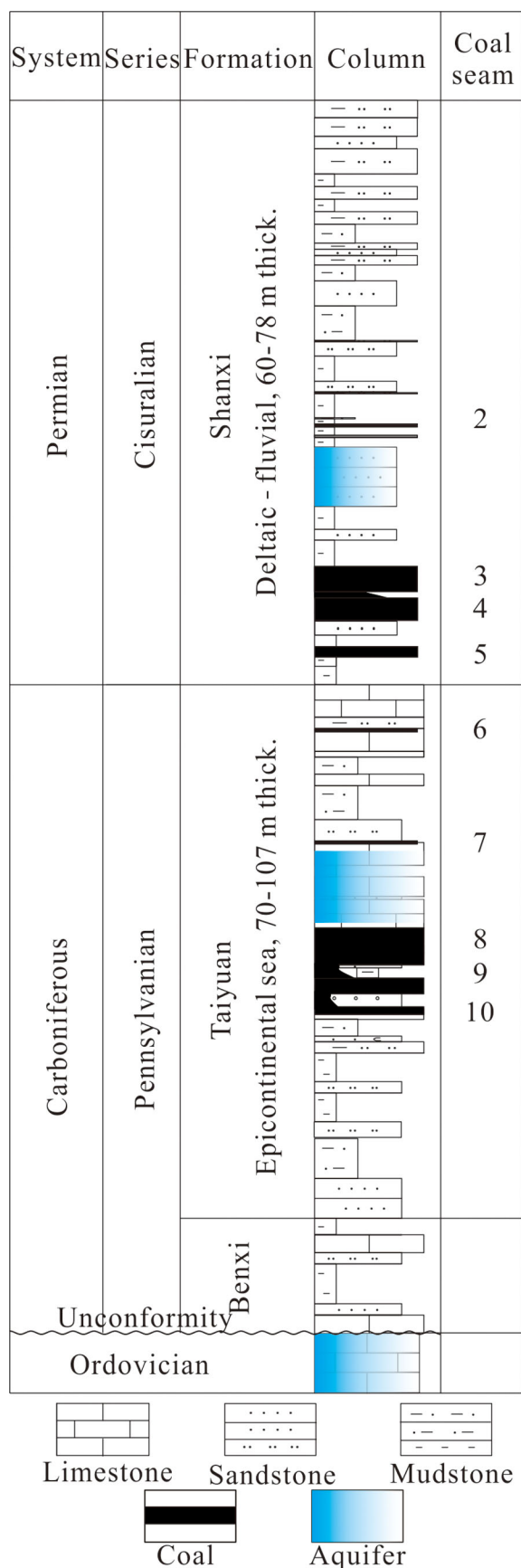
CBM exploration stagnated until the China United CBM Co. Ltd. started working in this region in the 2000s. The CBM production now shows great potential; 55 CBM production wells (52 vertical wells and 3 horizontal wells) were drilled by the end of 2012. The highest CBM production from the vertical wells is 2284 m<sup>3</sup>/d per well, and the highest daily production rate from horizontal wells is 9744 m<sup>3</sup>/d per well. Production varies considerably between coal seams and throughout the whole study area. The paper combines CBM geology, hydrogeology, CBM recovery and laboratory data to study CBM preservation and the mechanism by which groundwater affects CBM vertical well performance and provides recommendations for CBM recovery in the Liulin area. This detailed study, focused on water coproduced with CBM, may help to improve CBM

exploitation in the area and in similar regions around the world.

## GEOLOGICAL SETTING AND HYDROGEOLOGY

### Coal Stratigraphy

The geological evolution of the Liulin area was significantly influenced by the formation of the North China cratonic basin. The stratigraphy of the Eastern Ordos basin records the erosion from Silurian to Mississippian followed by the subsidence and sedimentation from the Pennsylvanian to the Triassic (Yao et al., 2009). Cambrian to Ordovician sediments are predominantly carbonates with subordinate amounts of siliciclastic sediments. Carboniferous to



Permian clastic sediments and coal seams disconformably overlie lower Paleozoic sediments. The main coal-bearing strata occur in the Taiyuan and Shanxi Formations of the Pennsylvanian and Cisuralian, respectively. The Taiyuan Formation records lagoonal, tidal flat, and sandbar depositional environments in an epicontinental sea; the precursor coal vegetation was present in a tidal flat environment following a marine regression. The Shanxi Formation was deposited in a fluvial-deltaic environment with the precursor coal vegetation occurring in delta plain deposits (Li et al., 2012). The splitting of coal seams was produced by the influx of sediments during sea-level fluctuations in the Taiyuan Formation, and the No. 8, 9, and 10 coal seams in the northwest split into three separate coal seams in most areas. The No. 3 and 4 coal seams were also split with the transition of depositional facies, showing a combination of No. 3 and 4 only in part of the middle and the north-east parts of the basin (Figure 1).

The Liulin area is located in the southern part of the Lishi Nose anticline, with a monoclinical structure striking roughly north-south and dipping to the west at 3–8°. Faulting is limited to the vicinity of the Jucaita Fault. Like other districts in North China, the Taiyuan Formation and Shanxi Formation are the main coal-bearing formations with almost nine coal seams (Figure 2). The main seams in the Taiyuan Formation are the No. 8, 9, and 10 seams, and those in the Shanxi Formation are the No. 3 and 4 and No. 5 coal seams. The relatively thick No. 3 and 4 (approximately 3–8 m [10–26 ft] thick) and No. 8 (approximately 3–10 m [10–33 ft] thick) coal seams became the main CBM development target during early CBM development. However, too much water was produced from the No. 8 coal seam for economic development because the seam was easily connected with its overlying limestone during hydraulic fracturing. The China United CBM Co. Ltd. chose to develop gas from separated coal seams. Thus, the target seams analyzed in this research include different combinations, e.g., No. 3 and 4, No. 9 and 10, and No. 3, 4, and 8. The coal burial depth ranges from 300 to 1100 m (984 to

**Figure 2.** Composite stratigraphic column showing coal-bearing formations in the Liulin area with the two aquifers associated with coal seams and the Ordovician limestone aquifer.

3609 ft). For examples, the No. 3 and 4 coal seam is only approximately 200 m (656 ft) deep in the north-east and gradually becomes deeper toward the south-west, with a maximum depth of 950 m (3117 ft).

## Hydrogeology

In the Liulin area, the mean annual precipitation is 506 mm (20 in.) with 60%–70% of the total precipitation falling in July, August, and September. The major rivers are the Qinglong and the Sanchuan. The ground surface elevation ranges from 660 to 1200 m (2165 to 3937 ft). The eastern part of the Liulin area is higher than the west; generally, the topography of the basin inclines to the west and southwest. On a regional scale, the Ordovician limestone and Quaternary sediment are hydraulically connected by the limestone outcrops in the east. However, the Permian and Carboniferous mudstones, shales, and siltstones interbedded with the aquifers develop as aquitards (Hao et al., 2006). Generally, there are six independent aquifers in the Ordovician to Quaternary strata of the Liulin area (Su et al., 2003), as follows: (1) the Middle Ordovician limestone karst-fractured aquifer; (2) the Pennsylvanian limestone karst-fractured aquifer in the Taiyuan Formation; (3) the Cisuralian sandstone aquifer in the Shanxi Formation; (4) the Cisuralian sandstone aquifer in the Shihezi Formation; (5) the Guadalupian–Triassic sandstone aquifer; and (6) the Holocene conglomerate and sand aquifer. The first three aquifers are shown in Figure 2. The strata between the No. 10 coal seam and the top of the Ordovician is approximately 50–60 m (164–197 ft) and mainly composed of mudstone, which is a good aquitard barring the Middle Ordovician limestone water. The mudstones between the other aquifers also act as separate aquitards.

## Methodology

Samples of coproduced water were collected from CBM wells in the Liulin area. The CBM wells generally have different completion intervals that target the No. 3 and 4 or No. 9 and 10 coal seams, whereas the early wells usually targeted the No. 3, 4, and 8 coal seams. The sampled wells were selected largely on the basis of the extent of field development, covering most areas of the CBM development region, and

required production time no less than 18 months. All of the water samples used in this study were collected from 20 CBM wells, shown in Figure 1. Furthermore, the sampled wells for fluid inclusion and coal property test are also shown in Figure 1.

Water samples were collected following the guidelines of Rice (2003). Wells were allowed to flow as much as possible (at least 18 months) before the water samples were collected to ensure flushing of the sample ports and collection of a representative sample. Most wells were pumped 24 hours a day to dewater the coal. Water was collected directly from the wellhead by attaching Tygon tubing to a port on the wellhead tee. The water was collected in a clean polyethylene carboy with a spigot that was rinsed prior to sampling. Clean sample bottles were rinsed with formation water at least twice prior to sample collection.

The water in the carboy was filtered through a 0.1 m filter using a peristaltic pump, Tygon tubing, and an acrylic filter holder. Polyethylene bottles for sampling cations were prewashed with a 10% solution of 1:1 nitric acid:sulfuric acid followed by rinsing with deionized water. Polyethylene bottles for sampling anions were prewashed with deionized water. Bottles for filtered samples were rinsed at least twice with filtered water before filling. Samples for determination of cations, deuterium, oxygen isotopes, and anions were collected from filtered water.

Cation and anion concentrations were determined using analysis for oil and gas field water procedures from the China Petroleum and Natural Gas Industry Standards (SY/T 5523-200). The accuracy and precision of field sampling and analyses were assessed by comparing values for field blanks, deionized water blanks, and duplicate samples (6% of total samples). Mean deviations between duplicate samples were generally less than 7% for cations and 5% for anions ( $\text{Cl}^-$  and  $\text{SO}_4^{2-}$ ).

Stable isotopes of D/H and  $^{18}\text{O}/^{16}\text{O}$  in the water were analyzed by a commercial laboratory and reported using delta notation ( $\delta$ ) relative to known standards (Vienna standard mean ocean water [VSMOW] for D/H and Vienna Peedee belemnite [VPDB] for  $^{18}\text{O}/^{16}\text{O}$ ). Delta values are reported as per mil (‰) and calculated by equation 1.

$$\delta(\text{‰}) = (R_x/R_s - 1) \times 1000 \quad (1)$$

where  $R$  is the ratio of the heavy to the light isotope (e.g.,  $^{18}\text{O}/^{16}\text{O}$ ),  $R_x$  is the ratio of the sample, and  $R_s$  is the ratio of the standard. Both VSMOW and VPDB have  $\delta$  values reported in ‰; therefore, a sample with a positive delta has more of the heavier isotope than the standard, and a sample with a negative delta value has less of the heavier isotope than the standard.

Fluid inclusions were collected from quartz overgrowths in sandstones and from cave sparry calcite and grain-recrystallized calcite in carbonates directly above coal seams in the Shanxi and Taiyuan Formations. They were tested for temperature of homogenization and salinity. The methods were guided by the determination of temperature for fluid inclusion in minerals protocol from China's Nuclear Industry Standards (EJ/T 1105-1999). The samples were tested using a LINKAM THMS 600 heating and freezing table in a laboratory at 20°C and 30% humidity, and part of the fluid compositions were tested by LABHR-VIS LabRAM HR800 microscopic laser Raman spectroscopy.

Following Chinese standard GB/T 19560-2004, methane adsorption isotherm experiments on 13 samples were performed. All coal samples were prepared by crushing and sieving to a size range of 0.18 to 0.25 mm (60–80 mesh), and 100–125 g was weighed for the moisture-equilibrium treatment. The moisture-equilibrium treatment was processed for at least four days for each sample. After these pretreatments, the coals were put into the sample cell of the IS-100 for the adsorption isotherm experiment. The experimental temperature and equilibrium pressure were 30°C and up to 10 MPa. Before the adsorption experiment, the ash yield and moisture contents of the coal were determined according to Chinese standard GB/T 212-2001.

The gas contents of coal seams in both the Shanxi Formation and the Taiyuan Formation were also analyzed in this study. The gas content data were obtained from gas content test reports, which were directly measured using the method of Waechter et al. (2004). The adsorption isotherm analyses of coal samples were used to estimate the gas content and saturation of the coals from CBM wells. The experimentally estimated gas content was derived from adsorption isotherm data by computing the gas

content at the present reservoir temperature and pressure conditions. The estimated gas content was calculated based on the following hypotheses (Saulsberry et al., 1996): (1) CBM is composed of 100%  $\text{CH}_4$  and (2) reservoir temperatures of 30°C are valid. Under these assumptions, the gas content can be calculated by the Langmuir equation 2.

$$G_E = (1 - A_d - M_d) \times V_L \times P_R / (P_R + P_L) \quad (2)$$

where  $M_d$  and  $A_d$  are the moisture content and ash yield obtained from the proximate analysis of coals;  $V_L$  and  $P_L$  are Langmuir volume (the maximum adsorption capacity) and Langmuir pressure from the methane adsorption isotherm experiment;  $P_R$  is reservoir pressure; and  $G_E$  is the estimated gas content or experimental maximum gas content. However, uncertainties exist when using  $G_E$ . The temperature used in the experiment is not the in-situation reservoir pressure, and the estimated gas content is based on the hypothesis that CBM is saturated with 100%  $\text{CH}_4$ . However, in reality, the in-situation gas is mainly  $\text{CH}_4$  with some  $\text{CO}_2$ ,  $\text{N}_2$  and other gases. Despite the uncertainties, the estimated gas content provides the best approximation of the in-place gas content, particularly for areas where no in-place gas content can be obtained (Yao et al., 2009).

The effects of hydrodynamics on CBM accumulation were determined by analyzing the water level, hydrogeology, and geochemical signature of formation water. To summarize the gas and water production trend, typical wells were chosen in section "Production Performance of CBM Wells" to illustrate the influence of hydrogeology on CBM development.

## RESULTS AND DISCUSSION

### Geochemical Signature of Coproduced Water

#### Variation in Water Composition since Gas Production

Formation water in coal seams is easily contaminated by drilling fluid, drilling mud, and fracturing fluid (Gentzis et al, 2009). In the first six months of gas production, the produced water was high in TDS (bicarbonate, chloride, and sodium), but the TDS decreased quickly as water was pumped from wells (sample well P5 in Table 1). The water was generally

**Table 1.** Composition of Water Samples from Well P5 Every Month since Gas Production Began

Months since Gas Production Began	Ca <sup>2+</sup> (mg/L)	Mg <sup>2+</sup> (mg/L)	Na <sup>+</sup> + K <sup>+</sup> (mg/L)	HCO <sub>3</sub> <sup>-</sup> (mg/L)	SO <sub>4</sub> <sup>-</sup> (mg/L)	Cl <sup>-</sup> (mg/L)	TDS (mg/L)
1	89.16	8.58	1378.34	666.99	37.04	2126.02	4210
2	48.25	6.75	905.23	584.48	25.02	1526.25	3120
3	28.17	5.98	714.91	553.88	22.72	798.08	2201
4	30.27	3.28	525.21	487.25	10.25	455.02	1530
5	6.18	2.18	484.50	297.76	8.23	324.47	1150
6	12.28	5.25	452.02	320.58	20.25	315.23	1380
7	8.98	3.87	388.82	671.36	39.10	233.62	1365
8	7.93	3.45	367.26	706.77	28.23	167.90	1305
9	8.05	2.95	352.15	710.25	30.27	125.45	1250
10	6.02	3.05	252.15	680.15	10.15	105.25	1058
11	8.23	2.75	310.05	685.25	25.15	119.25	1165
12	6.78	2.90	347.32	722.27	12.97	108.34	1230
13	10.50	3.55	394.14	702.77	12.25	175.25	1320
14	6.90	3.15	393.15	712.41	12.88	150.07	1295
15	7.85	2.95	387.25	700.01	20.85	158.25	1315
16	7.22	3.44	385.25	698.25	39.58	151.02	1307

rich in sodium. As more water was pumped from the coal seams, the contaminating cations and anions were gradually removed, and the chemistry of the produced water approached the composition of the primary water in the coal seams. Four to six months after gas production, the value of TDS, bicarbonate, chloride, and sodium continued to decrease. This water contains a mixture of sodium chloride and sodium bicarbonate, and the proportion of chloride continually decreases. At this time, the cation and anion abundances are fairly stable, and the water is dominated by sodium bicarbonate.

#### Water Composition in Coal Seams

The water samples were collected from wells that had been pumped for at least 18 months. The major elements and measured parameters in water coproduced with CBM are given in Table 2. The water is dominated by sodium as the major cation, with bicarbonate and chloride as the dominant anions, and is also generally distinguished by very low concentrations of sulfate. However, chemical analysis of the water reveals distinct differences among waters from the No. 3 and 4, No. 9 and 10 and No. 3, 4, and 8 coal seams in the study area. The TDS value of water from the No. 3 and 4 and No. 9 and 10 coal seams varies

from 5302–6846 mg/L and 4452–7009 mg/L. Samples from the No. 3, 4, and 8 coal seams have the lowest TDS values, with a minimum value of only 423 mg/L and an average value of 3480 mg/L. The sharp decrease in TDS values in water from the No. 8 coal seam reflects a much more active hydrodynamic system in the No. 8 seam than in the other coal seams.

The mean sodium concentrations are significantly different among these three coal seams. Cation exchange with clay minerals most likely accounts for the relatively low concentration of potassium versus sodium in the water (Van Voast, 2003), and the values are summed as Na<sup>+</sup> + K<sup>+</sup> in Table 2. The No. 9 and 10 coal seams show higher average sodium and potassium value (2249.84 mg/L) than either the No. 3 and 4 (1954.83 mg/L) or the No. 3, 4, and 8 (894.49 mg/L) coal seams. It can be seen that the sodium and potassium concentrations are significantly different between the No. 3 and 4 and No. 3, 4, and 8 coal seams, with a low value of 57.28 mg/L in the No. 3, 4, and 8 coal seams. Calcium, magnesium, and potassium are low relative to sodium, representing only approximately 4% of the total cations on an equivalence basis. Magnesium concentrations are low in the Liulin CBM waters, and it appears that

**Table 2.** Composition of Water Samples from CBM Wells in the Liulin Area

Well	Coal Seam	PH	Ca <sup>2+</sup> (mg/L)	Mg <sup>2+</sup> (mg/L)	Na <sup>+</sup> + K <sup>+</sup> (mg/L)	HCO <sub>3</sub> <sup>-</sup> (mg/L)	CO <sub>3</sub> <sup>2-</sup> (mg/L)	SO <sub>4</sub> <sup>2-</sup> (mg/L)	Cl <sup>-</sup> (mg/L)	TDS (mg/L)
G1	3&4	7.55	51.40	77.03	1886.75	1501.35	108.29	104.13	2156.69	5890
Y1	3&4	7.73	39.22	74.35	1984.63	1338.25	64.97	392.72	2209.25	6108
Y2	3&4	7.66	21.32	30.48	1909.25	1440.56	203.62	152.32	1893.58	5658
Y3	3&4	7.63	34.12	31.17	1778.50	1298.26	45.72	36.22	2070.25	5302
Y4	3&4	7.57	24.98	28.31	1836.86	1506.24	69.79	77.79	1953.90	5505
Y7	3&4	7.35	36.93	27.94	2364.18	1421.58	–	60.51	2929.13	6846
Y16	3&4	7.54	28.18	53.34	2024.76	1684.36	66.42	264.25	2080.54	6207
Y18	3&4	7.76	25.89	18.24	1853.75	1419.13	168.45	21.40	1921.16	5432
Y5	9&10	7.34	45.69	61.10	2363.60	1355.52	60.16	260.13	2858.48	7009
Y8	9&10	7.32	27.26	24.25	1420.19	1594.32	89.04	24.28	1268.42	4452
Y9	9&10	7.60	26.12	15.93	2965.73	0.00	1996.35	22.64	1180.27	6751
L1	3&4, 8	7.30	15.61	9.52	1240.44	2154.25	–	103.25	614.66	4165
L2	3&4, 8	7.45	11.65	8.38	1284.15	2242.32	–	2.15	606.27	4266
L3	3&4, 8	8.30	10.41	8.88	38.37	2481.21	–	0.00	536.87	4303
L4	3&4, 8	7.30	17.73	17.45	1530.47	2194.13	137.83	2.00	959.99	4862
L5	3&4, 8	6.70	15.82	10.00	1448.36	2347.18	–	3.24	836.15	4798
L6	3&4, 8	7.30	17.69	11.42	1345.28	2172.23	120.60	0.75	715.41	4385
P1	3&4, 8	8.34	6.53	3.09	809.79	155.56	20.03	2.06	332.69	2742
P3	3&4, 8	8.04	31.90	23.40	57.28	275.25	–	28.30	19.54	423
P5	3&4, 8	7.60	68.30	24.50	296.28	574.77	–	12.25	308.36	1382

carbonate equilibrium controls the concentrations of calcium and magnesium (Hem, 1985).

Chloride (average value of 2047.43 mg/L) is much more abundant than bicarbonate (averaging 1455.96 mg/L) in formation water from the No. 3 and 4 and No. 9 and 10 coal seams, and the difference is almost 600 mg/L (Table 2). When the No. 8 coal seam is included, the bicarbonate content (1621.88 mg/L) increases sharply and is much higher than chloride (547.78 mg/L) with a difference of 1074.10 mg/L, which is caused by water recharge from the roof of the No. 8 coal seam. In the coal roof, fresh-water plumes containing sodium and bicarbonate water with low TDS content extend from the structurally upturned margin into the interior of the basin, which is also observed in the Black Warrior basin (Pashin, 2007).

The composition of water coproduced in Liulin CBM wells is similar to other water produced from CBM wells in the San Juan, Black Warrior, and Powder River basin in Montana and Wyoming in that they tend to be dominantly sodium bicarbonate or

sodium bicarbonate-chloride water (Table 3). Knowledge of the composition and volume of groundwater is required to implement plans for management such as disposal, treatment, and beneficial use in compliance with governmental regulation. Comparison of the volume of water coproduced with CBM in different depositional environment basins shows that the marine-transitional environment may produce much more water than the continental environment (Flores, 2013).

#### Isotopic Composition

The  $\delta^2\text{H}$  and  $\delta^{18}\text{O}$  values of water have been used extensively in sedimentary basins to determine the origin and evolution of basin water (Kharaka and Carothers, 1986; Rice, 2003). The  $\delta^2\text{H}$  values for water from the CBM wells vary from  $-40.2\text{‰}$  to  $-71.8\text{‰}$ , with different coal seam combinations yielding different trends. Water from the No. 9 and 10 coal seams has the highest  $\delta^2\text{H}$  (averaging  $-45.2\text{‰}$ ); whereas, water from the No. 3 and 4 coal seams has the lowest value (averaging  $-61.1\text{‰}$ ).

**Table 3.** Summary Information for Typical Coalbed Methane-Producing Basins and Comparison with the Liulin Area

Basin	Formation	Depositional Environment	Coproducted		Water Rate (m <sup>3</sup> /day/well)	Source of Data
			Water Type	Water Type		
San Juan basin, southern Ute Reservation, Colorado	Upper Cretaceous Fruitland Formation	Continental-transitional	Na-HCO <sub>3</sub> -Cl	Na-HCO <sub>3</sub> -Cl	2-120 average 8	Kaiser et al. (1991) and Rogers and Rogers (1994)
Black Warrior basin, Alabama	Pennsylvanian Pottsville Formation	Continental-marine	Na-Cl-HCO <sub>3</sub> -	Na-Cl-HCO <sub>3</sub> -	1-180 average 18	Pashin et al. (1990) and Luckianow and Hall (1991)
Powder River basin, Montana and Wyoming	Paleocene Fort Union Formation	Continental	Na-HCO <sub>3</sub>	Na-HCO <sub>3</sub>	~60	Rice et al. (2000)
Raton basin, Colorado and New Mexico	Upper Cretaceous Vermejo Formation and Upper Cretaceous to Paleocene Raton Formation	Continental-transitional	Na-HCO <sub>3</sub>	Na-HCO <sub>3</sub>	~27.9	Flores (2013)
Uinta basin, Utah	Upper Cretaceous Ferron Sandstone Member	Continental-transitional	Na-HCO <sub>3</sub> -Cl	Na-HCO <sub>3</sub> -Cl	~5.7	Flores (2013)
Alberta basin, Wabamun area, Canada	Paleocene Paskapoo Formation	Continental	Na-SO <sub>4</sub> -HCO <sub>3</sub>	Na-SO <sub>4</sub> -HCO <sub>3</sub>	very little	Trudell and Faught (1987)
Ordos basin, Liulin, China	Pennsylvanian Taiyuan Formation, seam 8	Marine-transitional	Na-HCO <sub>3</sub> -Cl	Na-HCO <sub>3</sub> -Cl	~160	tested
Ordos basin, Liulin, China	Cisuralian Shanxi Formation, seam 3 and 4	Continental	Na-Cl-HCO <sub>3</sub>	Na-Cl-HCO <sub>3</sub>	~2	tested

**Table 4.** Hydrogen and Oxygen Isotopic Data from Formation Water in the Liulin Area

Sample Number	Coal Seam	TDS (mg/L)	$\delta^2\text{H}$ (‰)	$\delta^{18}\text{O}$ (‰)
Y1	3 and 4	6108	-52.9	-5.4
Y2	3 and 4	5658	-50.7	-5.0
Y16	3 and 4	6207	-71.8	-6.1
Y18	3 and 4	5432	-69.0	-5.7
Y8	9 and 10	4451	-50.2	-5.3
Y9	9 and 10	6751	-40.2	-4.5
P1	3, 4, and 8	2742	-64.6	-5.2
P3	3, 4, and 8	423	-61.7	-6.2

The trends in  $\delta^{18}\text{O}$  values are similar to those for deuterium to some extent;  $\delta^{18}\text{O}$  values vary from  $-6.2\text{‰}$  to  $-4.5\text{‰}$  with the lowest values in water from the No. 3 and 4 and No. 8 coal seams and the highest values in water from the No. 9 and 10 coal seams (Table 4).

As meteoric water interacts with the rock while flowing underground, deuterium values will increase, with the extent of change closely correlated with water-flow velocity. If the flow velocity is high, then the water-rock interaction time is short, and the difference in isotopes is small; in contrast, if the flow velocity is slow, then there is ample time for chemical interaction. A comparison of the isotopic characteristics between the formation water and meteoric water can, therefore, indicate the degree of connection between formation water and meteoric water. Liu et al. (2009) defined the northwestern China meteoric water line using the following formula:

$$\delta^2\text{H} = 7.24\delta^{18}\text{O} + 4.48 \quad (3)$$

where the  $\delta^2\text{H}$  and  $\delta^{18}\text{O}$  are all lower than the meteoric water line (Figure 3), which confirms that the ground water flows very slowly and was there for a very long time before meteoric water reached the sample site. The relatively negative  $\delta^2\text{H}$  values in the No. 9 and 10 coal seams are due to the longer flow distance and greater water-rock interaction time. The isotopic composition varies from heavier (enriched in deuterium) to lighter (depleted deuterium) values, suggesting mixing of new recharge or old basinal waters (Rice et al., 2008). The No. 9

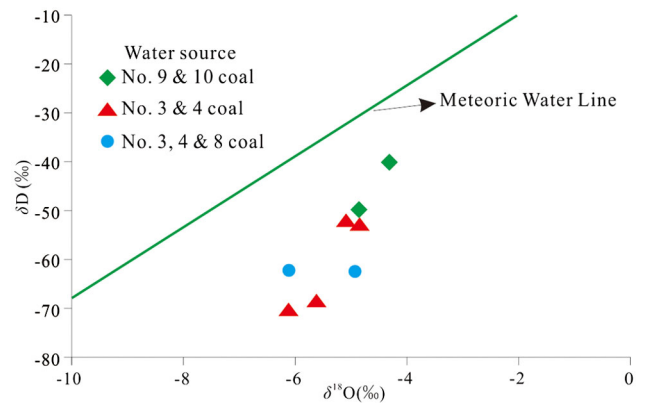
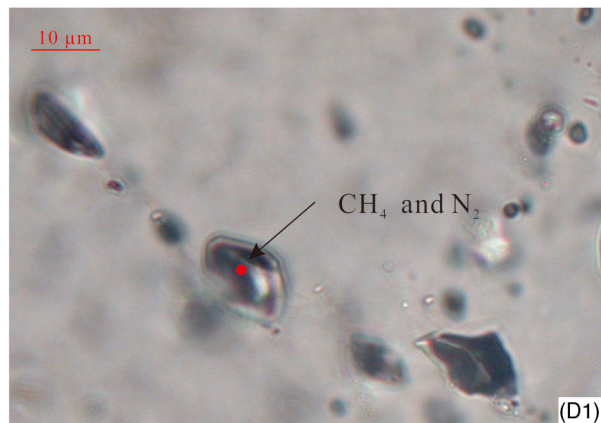
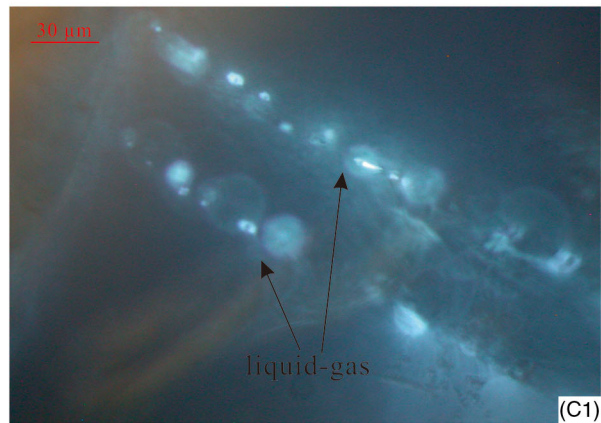
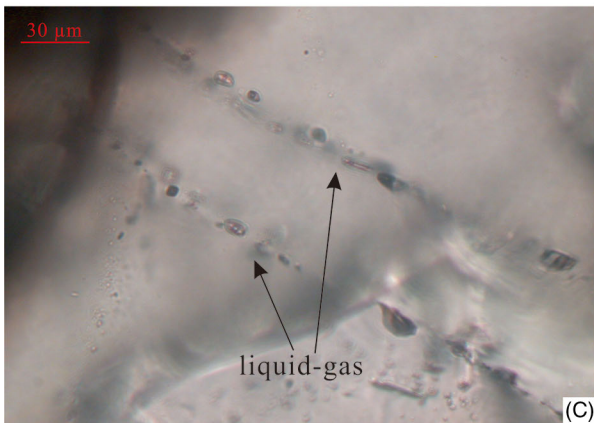
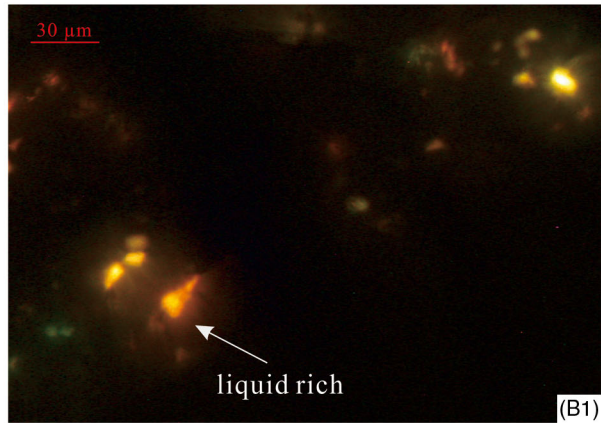
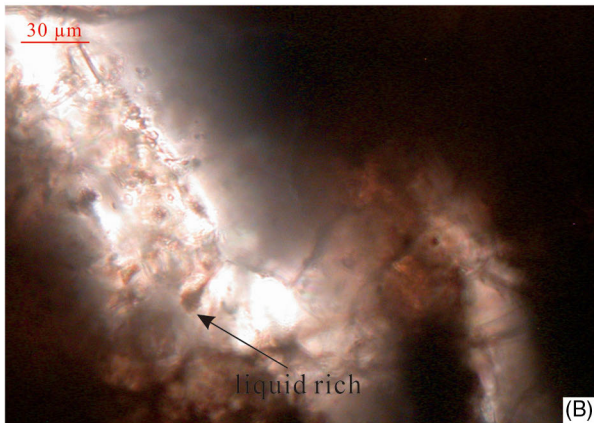
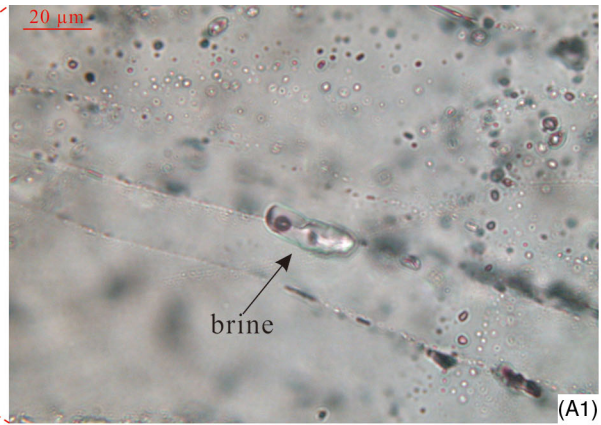
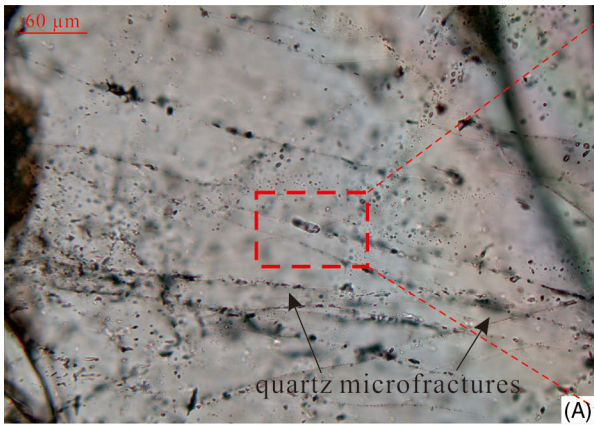


**Figure 3.** Plot of  $\delta\text{D}-\delta^{18}\text{O}$  for water coproduced with methane and its relation to the local meteoric water line in the Liulin area.

and 10 coal seams are relatively stable in water composition; whereas, waters from the No. 3, 4, and 8 coal seams may have been connected with new recharge or old basinal waters.

### Fluid Inclusions

Fluid inclusions in the roof of the coal seams in the Liulin area were divided into four types: brine, liquid hydrocarbon, liquid-gas hydrocarbon, and gas hydrocarbon inclusions (Figure 4). The inclusions occur in quartz overgrowth cement and microfracture trails on detrital quartz grain in the Shanxi Formation and in recrystallized limestone and solution holes filled in limestone in the Taiyuan Formation. These data show two stages of petroleum generation. The brine inclusions can be found along the quartz microfractures (Figure 4A) and are almost colorless or grayish (Figure 4A1). The liquid hydrocarbon fluids can be observed in calcite veins (Figure 4B) and have yellow-brown fluorescence with UV excitation. Strong blue fluorescence is shown for liquid-gas hydrocarbon fluids (Figure 4C1), while the fluids are mostly gray in visible light (Figure 4C). Raman spectroscopy was used to analyze the composition of the fluid, and the results show that the gas fluid is mainly  $\text{CH}_4$  and  $\text{N}_2$  (Figure 4D and D1). Two stages of petroleum fluids were classified based on the development position and host mineral characteristics of sandstone from the No. 3 coal seam roof or limestone overlying the No. 8 coal seam (Li et al., 2012). Further, based on the thermodynamic characteristics of the fluid inclusions,



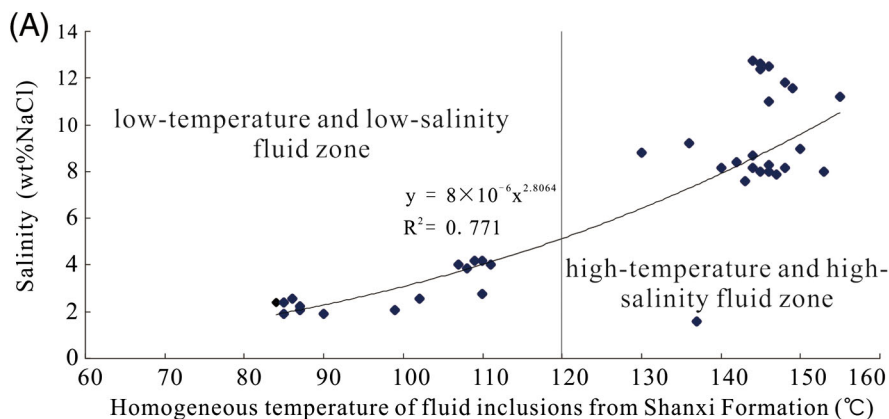
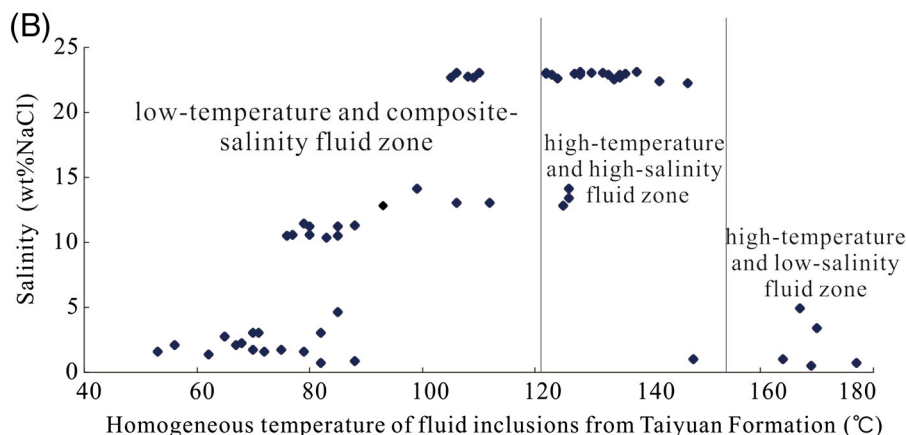


**Figure 5.** Classification of fluid inclusions captured in Shanxi Formation (A) and Taiyuan Formation (B) by homogenization temperature and salinity.



fluid from the Shanxi Formation was classified as either low-temperature and low-salinity fluid or high-temperature and high-salinity fluid, while fluids from the Taiyuan Formation were classified as low-temperature and composite-salinity fluid, high-temperature and high-salinity fluid, and high-temperature and low-salinity fluid (Figure 5 and Table 5).

Combining the analysis of fluid inclusion types, thermodynamic characteristics, and the geothermal evolution of the Liulin area, the first stage of the hydrocarbon charge or migration in the Liulin area occurred during the Middle to Late Triassic with a relatively small amount of hydrocarbon generation. The second stage, which was a major period of hydrocarbon generation, occurred during the Early Cretaceous with prolific gas inclusions and high hydrocarbon generation intensity (Li et al., 2012).

The high-temperature and low-salinity fluid captured in the No. 8 coal roof showed that during the gas generation stage, the upper strata was influenced by low-salinity groundwater. Thus, the coal may also have been affected by the low-salinity fluid through its connection with upper strata.

### Hydrogeological Model of CBM Accumulation

Outcrops of coal-bearing strata are located on the east side of the study area. The formation water is primarily sourced from meteoric water, which laterally recharges the aquifer from limestone located in the eastern part of the study area (Figure 6). The westward-dipping structural nose, topography, and precipitation control groundwater migration (Su et al., 2003).

**Figure 4.** Micrographs showing four types of fluid inclusions captured in the roof of the No. 3 and No. 8 coal seams. Brine inclusion developed in quartz microfractures (A), showing a single phase of aqueous inclusion (A1). Liquid hydrocarbon in visible light (B) and yellow fluorescence under UV light (B1). Liquid-gas hydrocarbon inclusions in visible light (B) and blue fluorescence under UV light. Gas hydrocarbon inclusions developed in line (D), and the gas inclusions consist of  $N_2$  and  $CH_4$  (D1) based on Raman spectroscopy.

**Table 5.** Fluid Inclusion Test Data for the Shanxi and Taiyuan Formations in the Liulin Area

Sample Number	Formation	Numbers	Host Mineral Occurrences	Distribution Type	Size ( $\mu\text{m}$ )	Vapor Liquid Ratio (%)	Homogenization Temperature ( $^{\circ}\text{C}$ )	Salinity (wt% NaCl)
P1	Taiyuan Formation	12	Cave sparry calcite	Ribbon	$4 \times 8$	$\leq 5\%$	82	0.71
			Cave sparry calcite	Ribbon	$3 \times 4$	$\leq 5\%$	88	0.88
			Cave sparry calcite	Ribbon	$4 \times 5$	$\leq 5\%$	148	1.05
			Cave sparry calcite	Ribbon	$10 \times 15$	$\leq 5\%$	164	1.05
			Cave sparry calcite	Ribbon	$5 \times 15$	$\leq 5\%$	170	3.39
			Cave sparry calcite	Ribbon	$10 \times 14$	$\leq 5\%$	79	1.57
			Grain recrystallized calcite	Group	$5 \times 5$	$\leq 5\%$	76	10.49
			Grain recrystallized calcite	Group	$4 \times 6$	$\leq 5\%$	77	10.61
			Grain recrystallized calcite	Group	$4 \times 4$	$\leq 5\%$	80	10.61
			Cave sparry calcite	Ribbon	$3 \times 7$	$\leq 5\%$	83	10.36
			Cave sparry calcite	Ribbon	$4 \times 6$	$\leq 5\%$	85	10.49
			Cave sparry calcite	Ribbon	$3 \times 9$	$\leq 5\%$	167	4.96
P2	Shanxi Formation	10	Quartz grains	Ribbon	$5 \times 10$	$\leq 5\%$	146	3.23
			Quartz grains	Ribbon	$4 \times 4$	$\leq 5\%$	166	11.70
			Quartz grains	Ribbon	$6 \times 8$	$\leq 5\%$	107	2.07
			Quartz grains	Ribbon	$5 \times 17$	$\leq 5\%$	149	12.85
			Quartz grains	Ribbon	$5 \times 6$	$\leq 5\%$	150	12.96
			Quartz grains	Ribbon	$4 \times 10$	$\leq 5\%$	151	13.07
			Quartz grains	Ribbon	$8 \times 10$	$\leq 5\%$	153	13.29
			Quartz grains	Ribbon	$2 \times 15$	$\leq 5\%$	140	9.08
			Quartz grains	Ribbon	$6 \times 20$	$\leq 5\%$	145	9.21
			Quartz grains	Ribbon	$10 \times 25$	$\leq 5\%$	148	9.34
P4	Shanxi Formation	10	Quartz overgrowths	Ribbon	$4 \times 6$	$\leq 5\%$	119	12.02
			Quartz overgrowths	Ribbon	$4 \times 5$	$\leq 5\%$	144	12.73
			Quartz overgrowths	Ribbon	$3 \times 5$	$\leq 5\%$	145	12.39
			Quartz overgrowths	Ribbon	$2 \times 4$	$\leq 5\%$	146	12.51
			Quartz overgrowths	Ribbon	$4 \times 4$	$\leq 5\%$	145	12.62
			Quartz overgrowths	Ribbon	$5 \times 20$	$\leq 5\%$	137	1.57
			Quartz overgrowths	Ribbon	$3 \times 4$	$\leq 5\%$	140	-
			Quartz overgrowths	Ribbon	$3 \times 7$	$\leq 5\%$	140	-
			Quartz grains	Ribbon	$6 \times 10$	$\leq 5\%$	110	4.18
Quartz grains	Ribbon	$6 \times 8$	$\leq 5\%$	111	4.03			

### Gas Content and Saturation

The gas content of coal seams from the Taiyuan Formation is higher than that in coal seams from the Shanxi Formation. The southeast part of the study area has the highest gas content in both the Shanxi and Taiyuan Formations. In most of the central and southern areas of both coal seams, the gas content is higher than  $10 \text{ m}^3/\text{t}$ , with a maximum value of

$20 \text{ m}^3/\text{t}$ . The coal seams of the Shanxi Formation in the northeast possess the lowest gas contents, ranging from  $5\text{--}9 \text{ m}^3/\text{t}$  (Figures 7, 8). Based on the distribution of gas, both the southern and central northern regions are favorable for CBM development.

To investigate the CBM saturation, the estimated gas contents were compared with the in-place gas content in the same seam. Notably, most of the gas

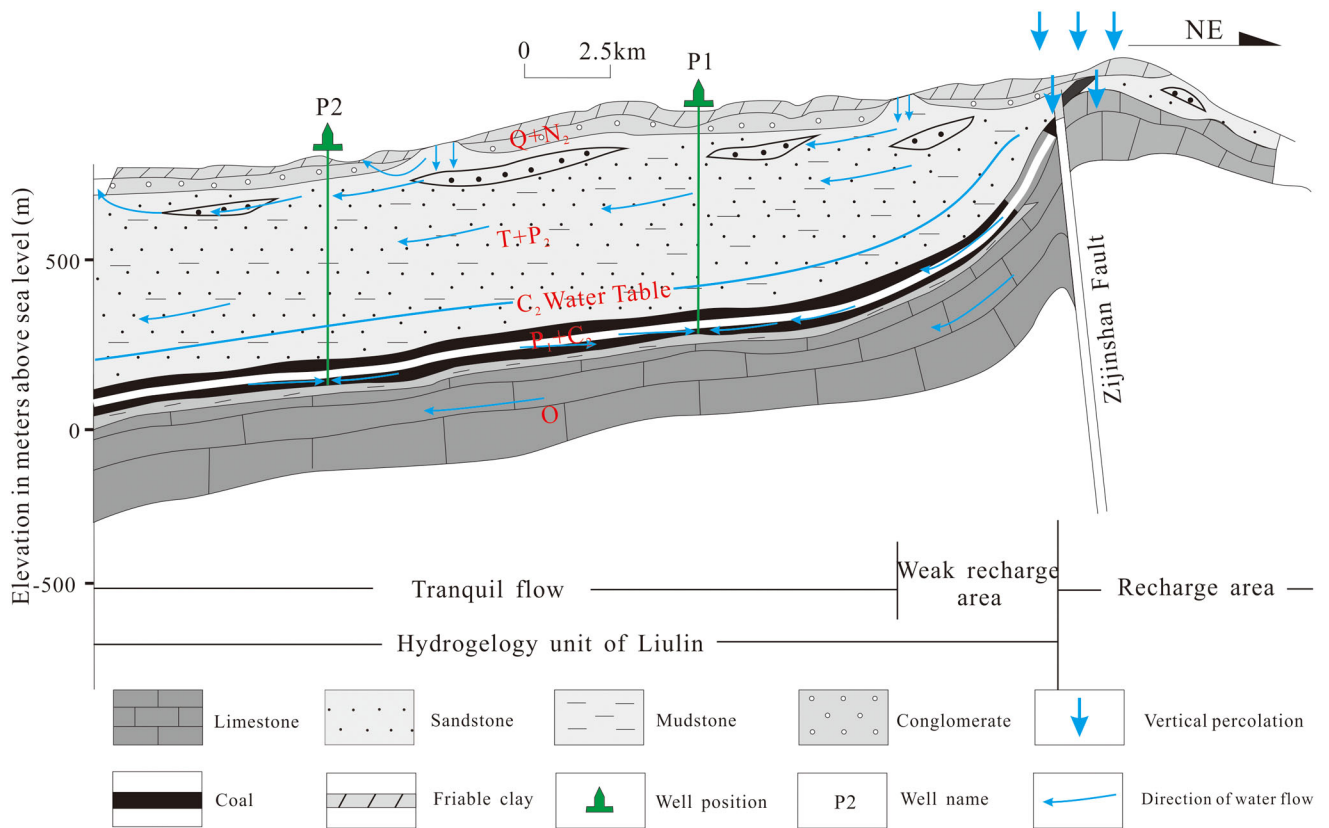


**Figure 6.** Simplified hydrogeological section of the Liulin area, showing the groundwater flow direction and classification of the recharge area, weak recharge area, and tranquil flow area.

in place is lower than the estimated gas content (Table 6) in both the No. 3 and 4 coal seams and No. 8 (8 and 9) coal seams, suggesting that these coal seams may be undersaturated (Drobnik et al., 2004). The undersaturation is more obvious in No. 8 coal seams where gas saturations calculated from the ratio of  $G_D/G_E$  averaged 63%, while the No. 3 and 4 coal seams averaged 72%.

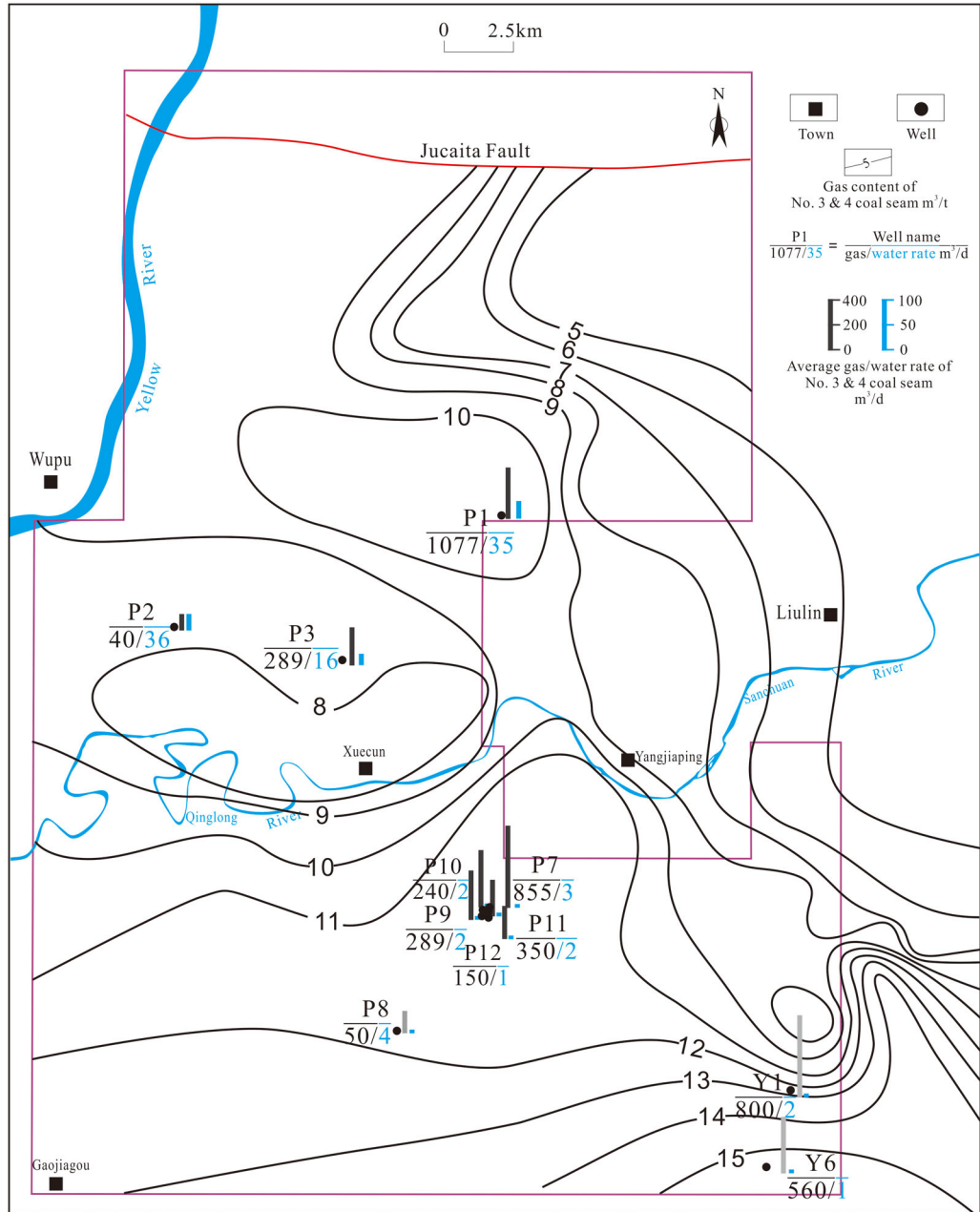
Various studies have identified the most important factors influencing methane storage and recovery, including coal type, rank, moisture content, mineral matter content, temperature, depth, natural fracturing, and stress (Laxminarayana and Crosdale, 1999). The coal seams in the Liulin area are found at depths of 300–900 m (984–2953 ft) and have little difference in coal type, rank, moisture content, and mineral matter content (Yao et al., 2009). Su et al. (2003) found that abnormally high pressure is present locally in the No. 8 coal reservoir. The groundwater moved CBM from the shallow coal seams into the deeper ones. Pressure increases with depth as does

gas content to such an extent that some coal seams in the north are actually over-pressured.

### Groundwater

The underground water in the Liulin area is from an independent hydrogeological unit separated from its adjacent areas. Groundwater recharge, flow, and discharge are predominantly controlled by topography. The six aquifers are independent of each other, and there is no hydraulic connection between them (Su et al., 2003). Groundwater in the strata above Shanxi Formation is mainly discharged through small springs with little groundwater flowing through faults along the northern margin of the Liulin area. Pump tests show that sandstones in the Shanxi Formation are easily drained, whereas limestone units in most of the wells in the Taiyuan Formation showed stable water flow caused by the continuous water supply from the limestone of the Taiyuan Formation. The influence radii of the limestone ranges from 14–51 m (46–167 ft), while the No. 8 coal seam is only

**Figure 7.** Gas content of the No. 3 and 4 coal seams and the gas/water average production rate for typical wells.



approximately 3–10 m (10–33 ft) thick. Thus, the water in the limestone may affect the gas accumulation and extraction from the underlying coal seams.

### Temperature of Coal Seams

The temperature of coal seams, determined by log data from uncased wells, can also reflect how enclosed the CBM reservoir is. Coal seams No. 3 and 4 and No. 8 are notably similar in temperature. In general, the deeper a reservoir is, the higher the temperature is. In the Liulin area, however, coal

seams No. 3 and 4 range from 19.64 to 35.1°C, and No. 8 ranges between 21.39 and 33.63°C (Figure 9). The temperature of the deeper No. 8 coal seam is not higher than the No. 3 and 4 coal seams and is even lower in some areas, indicating the possibility of fluid connections between the coal seams and aquifers.

### Gas Pressure Sealing Model for the Shanxi Formation

The roof of the No. 3 and 4 coal seams in the Shanxi Formation is mainly composed of mudstone with

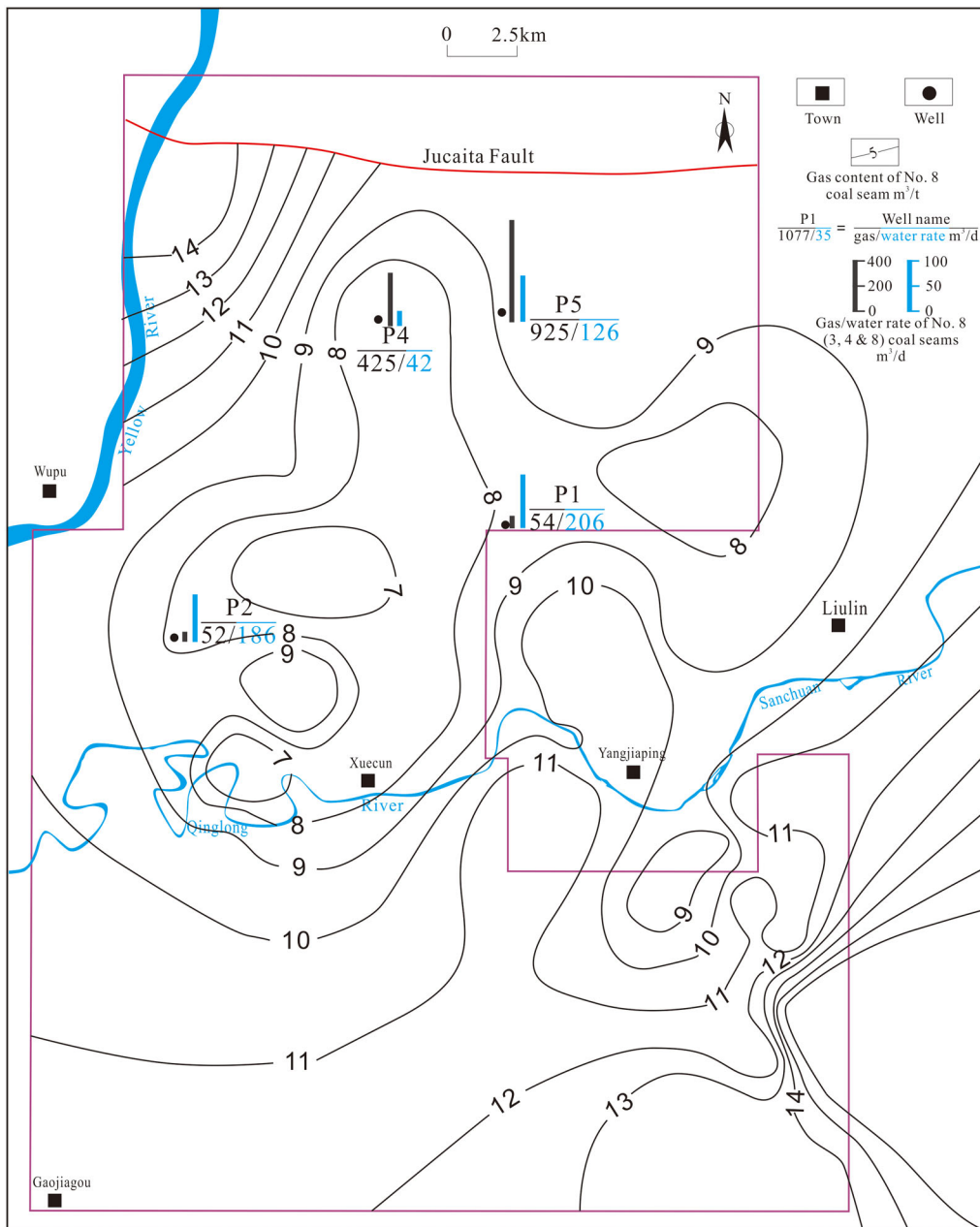


**Figure 8.** Gas content of the No. 8 coal seam and the gas/water average production rate for typical wells.

minor siltstone. The gas volume of the coal seam roof is relatively low, although certain areas contain some formation water in sandstone fractures. In general, there are no hydrodynamic migration or dissipation effects, and the gas saturation of the coal is higher than that of the Taiyuan Formation. The roof of the No. 3 and 4 coal seams is effectively a cap rock, and gas could be constricted in coal with a relatively high gas content. In such a situation, burial depth is the main factor affecting gas content. The gas production rate is relatively high when the roof is sandstone,

which may be caused by gas storage in the sandstone; whereas, the water production rate shows no regular pattern as the coal depth increases (Figure 10).

#### Hydrostatic Pressure Sealing Model for the Taiyuan Formation

The water recharge area and discharge area are located outside the study area (Figure 11). Within the study area, the formation water is mostly in a state of weak flow and stagnant, which is beneficial for CBM preservation. From northeast to southwest, the

**Table 6.** Methane Isothermal Adsorption Measurements and the Estimated Gas Content and Gas Saturation\*

Coal Seam	Sample Number	Depth (m)	$M_d$ (%)	$A_d$ (%)	EM (%)	$V_L$ (m <sup>3</sup> /t)		$P_L$ (MPa)	$P_R$ (MPa)	$G_E$ (m <sup>3</sup> /t)	$G_D$ (m <sup>3</sup> /t)	Saturation (%)
						As-Received	DAF					
3 and 4	P1	486	0.56	0.42	6.87	20.91	22.31	2.25	2.91	11.68	11.46	0.98
	P5	579	0.64	9.79	13.58	20.94	23.36	3.52	2.58	7.93	6.62	0.83
	G27	760	0.46	18.92	21.88	18.37	22.73	2.45	8.33	11.44	2.72	0.24
	G36	711	0.61	22.81	7.19	22.06	28.76	2.79	7.49	12.31	13.03	1.06
	D1	495	0.89	3.52	8.14	22.45	23.48	1.79	4.39	15.24	9.93	0.65
	D2	878	0.78	6.97	10.25	21.59	23.38	2.29	6.36	14.64	7.93	0.54
	average	652	0.66	10.41	11.32	21.05	24.00	2.52	5.34	12.21	8.62	0.72
8/8 and 9	P1	539	0.42	15.23	5.38	23.20	27.86	2.04	3.66	12.57	8.51	0.68
	P2	1105	0.40	23.78	5.99	18.75	24.05	2.60	9.30	11.11	7.42	0.67
	P5	642	5.91	17.47	6.97	25.53	27.30	1.67	3.31	13.00	10.25	0.79
	G27	834	0.47	12.25	12.42	25.54	29.22	1.97	8.48	18.09	5.36	0.30
	G36	783	0.64	15.47	5.92	16.10	19.16	3.18	8.25	9.75	11.87	1.22
	D1	556	0.68	15.32	6.46	22.34	26.56	1.55	4.82	14.20	6.74	0.47
	D2	928	0.72	4.01	11.68	23.53	24.68	1.76	6.78	17.80	5.14	0.29
average	770	1.32	14.79	7.83	22.14	25.55	2.11	6.37	13.79	7.90	0.63	

\* $M_d$  = moisture content (% air dry base),  $A_d$  = ash yield (% air dry base), EM = equilibrium moisture content (%), DAF = dry as free,  $V_L$  = Langmuir volume (m<sup>3</sup>/t),  $P_L$  = Langmuir pressure (MPa),  $P_R$  = approximate reservoir pressure (MPa),  $G_E$  = estimated gas content from the equation  $G_E = (1 - A_d - M_d) \times V_L \times P_R / (P_R + P_L)$ ,  $G_D$  = in-place gas content (m<sup>3</sup>/t), Saturation = percentage of  $G_D / G_E$  (%).

burial depth, reservoir pressure, and gas content increase. In the southwestern part of the district, the flow rate of underground water is much lower, which is theoretically beneficial for CBM accumulation and preservation. However, although it contains a considerable amount of gas, the amount of water in the Taiyuan Formation coal seams and recharge rate are much too high for favorable CBM

production because of high reservoir pressure, poor drainage, and the inability to lower the pressure during CBM development. In addition, the coal seams appear to split and thin. Thus, the central and eastern areas should be favorable regions for CBM development.

### Production Performance of CBM Wells

Wells P1 and P5 were completed in the No. 3, 4, and 8 coal seams. In the early stages, the gas production rate was much too low, and water production was very high (peak rates as much as 200 m<sup>3</sup>/d). In addition, the fluid levels could not be lowered (Figure 12). Later, well P1 shut out the No. 8 coal seam and only produced gas from the No. 3 and 4 seam. The water production rate later declined quickly, with the volume dropping to less than 25 m<sup>3</sup>/d. Well P5, however, did not exhibit the same changes, and water production remained high. Although gas production in P5 was much higher than in P1 (up to 1000 m<sup>3</sup>/d), the production efficiency was not good because of the high water production volumes. Well

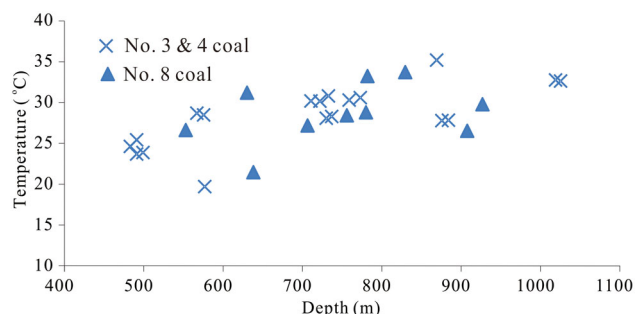


**Figure 9.** Temperature of the coal seams as a function of burial depth in the Liulin area. Note that the temperature of the No. 8 coal seam is even lower than that of the No. 3 and 4 coal seam at some depths.

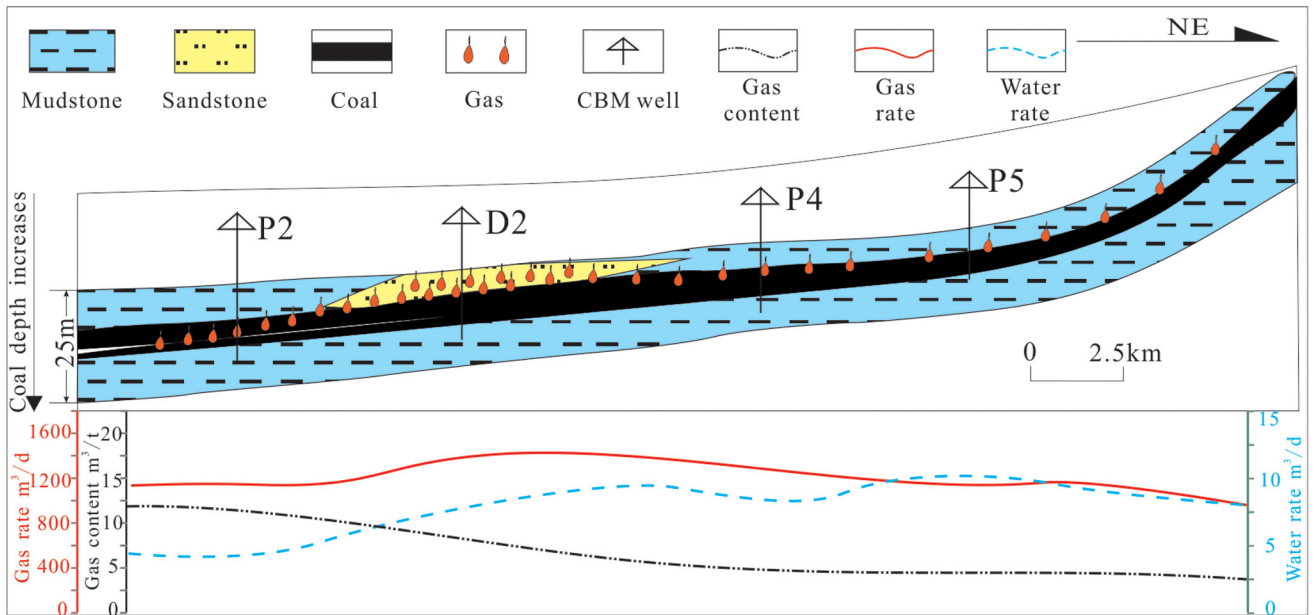


**Figure 10.** Gas pressure sealing model for the Shanxi Formation compared with the gas rate, water rate, and gas content variation of the coal seams.

Y2 only produced gas from the No. 3 and 4 coal seam, and water production was notably low ( $<10 \text{ m}^3/\text{d}$ ). The water production rate for Y9 completed in the No. 9 and 10 coal seams was only approximately  $1\text{--}2 \text{ m}^3/\text{d}$ . The production data all

indicated that coal seam No. 8 contributed to the high rates of water production.

Gas production increased quickly in Well P1 for two main reasons: (1) the water was not connected between the No. 8 coal seam and the upper limestone

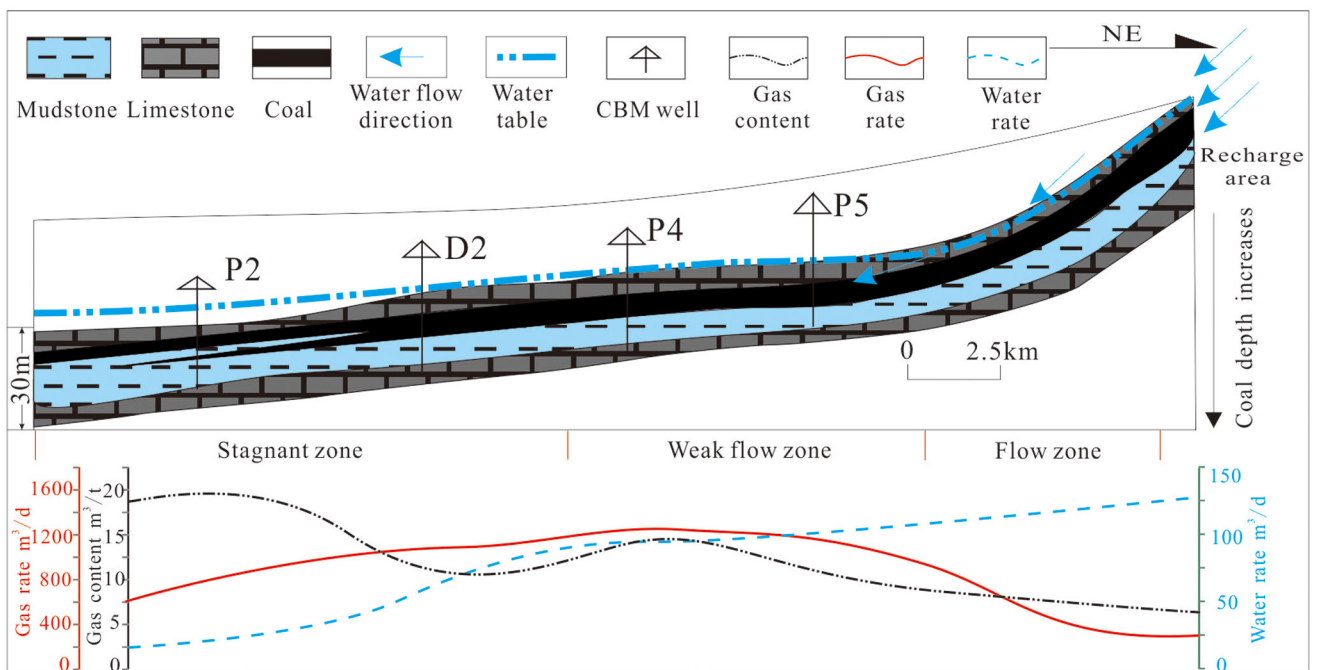


**Figure 11.** Hydrostatic pressure sealing model for the Taiyuan Formation compared with the gas rate, water rate, and gas content variation of the coal seams.

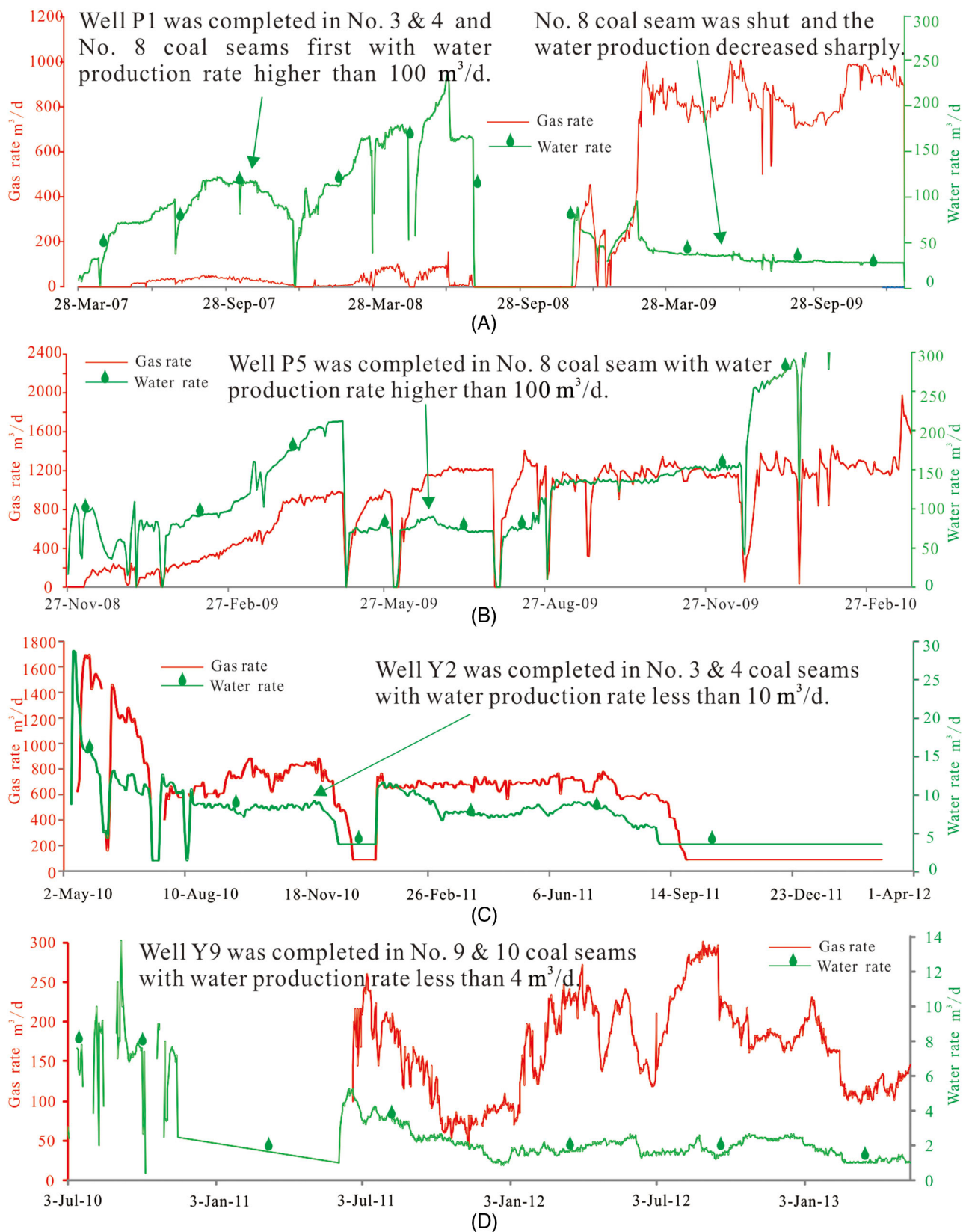


**Figure 12.** Gas and water production for wells completed in different coal seams, showing that the No. 8 coal seam is the main source of the large volume of water production (A and B), while the No. 3 and 4 (C) and No. 9 and 10 (D) coal seams produce small amounts of water.

unit, and (2) the sandstone aquifer in the Shanxi Formation does not allow water to flow through it efficiently. Comparatively, it is easier to lower the pressure of the well in the eastern part of the area and, therefore, obtain higher production. Combined with production data from other wells, it was concluded that it is important to avoid a connection with an aquifer when choosing an exploitation method. For vertical wells, regardless of whether both the No. 3 and 4 and No. 8 coal seams are exploited or only the No. 8 coal seam, the gas production was lower than expected. The main reason for this reduced production is that when developing CBM from the No. 8 seam, it is easy to create a connection with limestone aquifers, resulting in large volumes of water production, high bottomhole flowing pressure, and an inability to reduce reservoir pressure by lowering levels of water.

## CONCLUSIONS

In the Liulin area, the principal target seams for CBM development include the No. 3 and 4 coal seams in the sandstone Shanxi Formation, and the No. 8 (sub-jacent-karst) and No. 9 and 10 mudstone-bounded seams in the Taiyuan Formation. Geological and hydrodynamic mechanisms are two key controls of gas accumulation and production. There are a total of six aquifers in the Ordovician to Quaternary sequence, with the limestone karst/fractured aquifer in the Taiyuan Formation connected closely with the No. 8 coal seam. The TDS content of comingled formation waters from the No. 3 and 4 and the No. 8 coal seams is much lower than that derived from the separately sampled No. 3 and 4 or No. 9 and 10 seams. High TDS contents of the No. 9 and 10 coal seams suggest a more stagnant environment than the No. 8 coal seam, which is in an active hydrological environment, as demonstrated by water composition, H/O isotopes, and fluid inclusions trapped in the roof strata of the coal seams. Coproduced water in different coal seams shows that the composition is affected both by the original depositional setting of the coal as well as mixing and flushing of groundwater from the recharge area downstream. This is also observed in the San Juan, Black Warrior, Powder River, and

Piceance basins. This paper analyzes fluid inclusions as an indicator of the hydraulic connection between the coal seam reservoir and the overlying strata during its burial history together with water production rates and reservoir temperatures as an indication of current hydraulic connections. This latter condition is a significant factor relating to associated high rates of water production during current CBM development.

Consistent with observations, two CBM accumulation models are proposed that focus on CBM produced from either continental or marine-transitional strata, respectively. These relate to gas pressure sealing in the sandstone Shanxi Formation (continental) and hydrostatic pressure sealing in the subjacent-karst and mudstone Taiyuan Formation (marine-transitional) based on gas content and on rates of gas and water recovery. Gas pressure sealing requires a stable coal roof with the gas content increasing with increased burial depth of the coal. Hydrodynamic sealing results where the advective flux of water into the reservoir directly balances the buoyant and dissolved flux of gas within counter-migrating fluids. Thus the migration of desorbed gas to low-pressure areas is obstructed by formation fluids. Furthermore, this restricts the desorption of CBM from coal, thereby keeping the gas in the coal.

The monocline CBM reservoir of the Shanxi and Taiyuan Formations is a typical CBM reservoir pattern, and the coproduced water volume and chemical characteristics are also common in different depositional environments and stratigraphically combined basins. The water production rate of wells only completed in the No. 3 and 4 coal seams is less than  $10 \text{ m}^3/\text{d}$ , and that of those in the No. 9 and 10 seams is only  $1\text{--}2 \text{ m}^3/\text{d}$ . However, the water production rate may reach  $200 \text{ m}^3/\text{d}$  in the No. 8 coal seam. The characteristics of the high pressure, high gas content, monocline reservoir model of the No. 8 coal seam are similar to those of the northern part of San Juan basin. However, the problem of high water production rates must be solved in order to obtain high and stable CBM production in the Liulin area. In such situations, better gas production can potentially be achieved by drilling lateral wells or by avoiding the No. 8 coal seam in vertical wells—but with the disadvantage of wasting a significant resource.

## REFERENCES CITED

- Ayers, W. B., 2002, Coalbed gas systems, resources, and production and a review of contrasting cases from the San Juan and Powder River Basins: AAPG Bulletin, v. 86, p. 1853–1890.
- Bachu, S., and K. Michael, 2003, Possible controls of hydrogeological and stress regimes on the producibility of coalbed methane in Upper Cretaceous-Tertiary strata of the Alberta basin, Canada: AAPG Bulletin, v. 87, no. 11, p. 1729–1754, doi:10.1306/06030302015.
- Cai, Y., D. Liu, Y. Yao, J. Li, and Y. Qiu, 2011, Geological controls on prediction of coalbed methane of No. 3 coal seam in Southern Qinshui Basin, North China: International Journal of Coal Geology, v. 88, no. 23, p. 101–112, doi:10.1016/j.coal.2011.08.009.
- Drobniak, A., M. Mastalerz, J. Rupp, and N. Eaton, 2004, Evaluation of coalbed gas potential of the Seelyville Coal Member, Indiana, USA: International Journal of Coal Geology, v. 57, no. 34, p. 265–282, doi:10.1016/j.coal.2003.12.007.
- Dubessy, J., S. Buschaert, W. Lamb, J. Pironon, and R. Thiéry, 2001, Methane-bearing aqueous fluid inclusions: Raman analysis, thermodynamic modelling and application to petroleum basins: Chemical Geology, v. 173, p. 193–205.
- Flores, R. M., 2013, Coal and Coalbed Gas: Fueling the Future: Coal and Coalbed Gas: Amsterdam, Elsevier Science, 720 p.
- Gentzis, T., N. Deisman, and R. J. Chalaturnyk, 2009, Effect of drilling fluids on coal permeability: Impact on horizontal wellbore stability: International Journal of Coal Geology, v. 78, p. 177–191.
- Hao, Y., T.-C. J. Yeh, Z. Gao, Y. Wang, and Y. Zhao, 2006, A gray system model for studying the response to climatic change: The Liulin karst springs, China: Journal of Hydrology, v. 328, p. 668–676.
- Hem, J. D., 1985, Study and interpretation of the chemical characteristics of natural water, 3rd ed.: U. S. Geological Survey Water Supply Paper 2254, 263 p.
- Kaiser, W. R., T. E. Swartz, and G. J. Hawkins, 1991, Hydrology of the Fruitland Formation, San Juan basin, in Geologic and hydrologic controls on the occurrence and productivity of coalbed methane, Fruitland Formation, San Juan basin: Gas Research Institute Topical Report GRI-91/0072, p. 195–241.
- Kaiser, W. R., D. S. Hamilton, A. R. Scott, R. Tyler, and R. J. Finley, 1994, Geological and hydrological controls on the producibility of coalbed methane: Journal of the Geological Society, v. 151, no. 3, p. 417–420, doi:10.1144/gsjgs.151.3.0417.
- Karacan, C. Ö., F. A. Ruiz, M. Cotè, and S. Phipps, 2011, Coal mine methane: A review of capture and utilization practices with benefits to mining safety and to greenhouse gas reduction: International Journal of Coal Geology, v. 86, no. 23, p. 121–156, doi:10.1016/j.coal.2011.02.009.
- Kharaka, Y. K., and W. W. Carothers, 1986, Oxygen and hydrogen isotope geochemistry of deep basin brines, in P. Fritz and J. Ch. Fontes, eds., Handbook of Environmental Isotope Geochemistry: The terrestrial environment, B: Amsterdam, Elsevier Scientific Publishing Company, p. 305–360.
- Lamarre, R. A., 2003, Hydrodynamic and stratigraphic controls for a large coalbed methane accumulation in Ferron coals of east-central Utah: International Journal of Coal Geology, v. 56, no. 12, p. 97–110, doi:10.1016/S0166-5162(03)00078-8.
- Laxminarayana, C., and P. J. Crosdale, 1999, Role of coal type and rank on methane sorption characteristics of Bowen Basin, Australia coals: International Journal of Coal Geology, v. 40, no. 4, p. 309–325, doi:10.1016/S0166-5162(99)00005-1.
- Li, Y., D. Tang, H. Xu, H. Li, and S. Tao, 2012, Evolution of coal-derived hydrocarbon based on the analysis of fluid inclusions in the Permo-Carboniferous strata of Liulin area in the Ordos Basin: Geological Journal of China Universities, v. 18, p. 419–426 (in Chinese with an English abstract).
- Liu, J., X. Song, G. Yuan, X. Sun, X. Liu, and S. Wang, 2009, Characteristics of  $\delta^{18}\text{O}$  in precipitation over Eastern Monsoon China and the water vapor sources: Chinese Science Bulletin, v. 55, p. 200–211.
- Luckianow, B. J., and W. L. Hall, 1991, Water storage key factor in coalbed methane production: Oil & Gas Journal, v. 89, March 11, 1991, p. 79–84.
- Norinaga, K., H. Kumagai, J. Hayashi, and T. Chiba, 1997, Type of water associated with coal: Fuel Chemistry, v. 42, p. 238–243.
- Pashin, J. C., 2007, Hydrodynamics of coalbed methane reservoirs in the Black Warrior Basin: Key to understanding reservoir performance and environmental issues: Applied Geochemistry, v. 22, p. 2257–2272.
- Pashin, J. C., 2010, Variable gas saturation in coalbed methane reservoirs of the Black Warrior Basin: Implications for exploration and production: International Journal of Coal Geology, v. 82, p. 135–146.
- Pashin, J. C., W. E. Ward, II, R. B. Winston, R. V. Chandler, D. E. Bolin, R. P. Hamilton, and R. M. Mink, 1990, Geologic evaluation of critical production parameters for coalbed methane resources: part II: Black Warrior basin: Gas Research Institute Annual Report GRI-90/0014.2, 190 p.
- Rice, C. A., M. S. Ellis, and J. H. Bullock Jr., 2000, Water coproduced with coalbed methane in the Powder River basin, Wyoming: preliminary compositional data: U.S. Geological Survey Open-File Report 00-372, 22 p.
- Rice, C. A., 2003, Production waters associated with the Ferron coalbed methane fields, central Utah: chemical and isotopic composition and volumes: International Journal of Coal Geology, v. 56, p. 141–169.
- Rice, C. A., R. M. Flores, G. D. Stricker, and M. S. Ellis, 2008, Chemical and stable isotopic evidence for water/rock interaction and biogenic origin of coalbed methane, Fort Union Formation, Powder River Basin, Wyoming and Montana U.S.A: International Journal of Coal Geology, v. 76, no. 12, p. 76–85, doi:10.1016/j.coal.2008.05.002.
- Rogers, R. E., and R. E. E. Rogers, 1994, Coalbed methane: Principles and practice: Michigan, PTR Prentice Hall, 345 p.
- Saulsberry, J. L., P. S. Schafer, and R. A. Schraufnagel, 1996, A guide to coalbed methane reservoir engineering: Gas Research Institute Report GRI-94/0397, 345 p.

- Scott, A. R., 2002, Hydrogeologic factors affecting gas content distribution in coal beds: *International Journal of Coal Geology*, v. 50, no. 14, p. 363–387, doi:[10.1016/S0166-5162\(02\)00135-0](https://doi.org/10.1016/S0166-5162(02)00135-0).
- Scott, A. R., W. R. Kaiser, and W. B. Ayers, 1994, Thermogenic and secondary biogenic gases, San Juan Basin, Colorado and New Mexico; implications for coalbed gas producibility: *AAPG Bulletin*, v. 78, p. 1186–1209.
- Song, Y., M. Zhao, F. Hong, S. Liu, and S. Qin, 2010, Pool-Forming Stages and Enrichment Models of Medium- to High-Rank Coalbed Methane: *Acta Geologica Sinica*, v. 84, no. 2, p. 382–405, doi:[10.1111/j.1755-6724.2010.00151.x](https://doi.org/10.1111/j.1755-6724.2010.00151.x).
- Su, X., L. Zhang, and R. Zhang, 2003, The abnormal pressure regime of the Pennsylvanian No. 8 coalbed methane reservoir in Liulin–Wupu District, Eastern Ordos Basin, China: *International Journal of Coal Geology*, v. 53, no. 4, p. 227–239, doi:[10.1016/S0166-5162\(03\)00015-6](https://doi.org/10.1016/S0166-5162(03)00015-6).
- Tao, S., Y. Wang, D. Tang, H. Xu, Y. Lv, W. He, and Y. Li, 2012, Dynamic variation effects of coal permeability during the coalbed methane development process in the Qinshui Basin, China: *International Journal of Coal Geology*, v. 93, p. 16–22, doi:[10.1016/j.coal.2012.01.006](https://doi.org/10.1016/j.coal.2012.01.006).
- Trudell, M. R., and R. Faught, 1987, Premining groundwater conditions at the Highvale site: Alberta Land Conservation and Reclamation Council Report Reclamation Research Technical Advisory Committee, Alberta, 83 p.
- Waechter, N. B., G. L. Hampton, III, and J. C. Shipps, 2004, Overview of coal and shale gas measurement: field and laboratory procedures, *in* 2004 International Coalbed Methane Symposium: University of Alabama, Tuscaloosa, Alabama, 17 p.
- Van Voast, W. A., 2003, Geochemical signature of formation waters associated with coalbed methane: *AAPG Bulletin*, v. 87, no. 4, p. 667–676, doi:[10.1306/10300201079](https://doi.org/10.1306/10300201079).
- Yao, Y., D. Liu, D. Tang, S. Tang, Y. Che, and W. Huang, 2009, Preliminary evaluation of the coalbed methane production potential and its geological controls in the Weibei Coalfield, Southeastern Ordos Basin, China: *International Journal of Coal Geology*, v. 78, no. 1, p. 1–15, doi:[10.1016/j.coal.2008.09.011](https://doi.org/10.1016/j.coal.2008.09.011).